Meteorological Applications

RMetS Royal Meteorological Society

RESEARCH ARTICLE OPEN ACCESS

Analysis and Simulations for the Severe Turbulence Event Aloft Myanmar on 21 May 2024

Christy Yan Yu Leung[1] | Haoming Chen[2] | Xiaoming Shi[2] | Ping Cheung[1] | Pak Wai Chan[1]

[1]Hong Kong Observatory, Hong Kong, China | [2]Hong Kong University of Science and Technology, Hong Kong, China

Correspondence: Christy Yan Yu Leung (yyleung@hko.gov.hk)

Received: 5 November 2024 | **Revised:** 6 May 2025 | **Accepted:** 9 May 2025

Funding: This work was supported by the World Meteorological Organisation and the Research Grant Council of Hong Kong SAR, China (HKUST-16301322).

Keywords: aviation safety | aviation turbulence | convectively induced turbulence | flight incident | model simulation | severe turbulence

ABSTRACT

A severe turbulence event was encountered by Singapore airlines SQ321 on 21 May 2024 over Myanmar which led to one fatality and multiple injuries. Analysis of ADS-B data indicated the event happen during the cruising phase of flight over the Irrawaddy Delta, Myanmar. Fluctuations in the vertical speed induced large vertical acceleration and indicated a severe magnitude of aviation turbulence. A study on the satellite and lightning data hinted that the turbulence was likely related to convectively induced turbulence on the downwind side of developing convective clouds. Simulation using Model for Prediction Across Scales (MPAS) with convective permitting resolution indicated the development of convective cells along the coast, moderate turbulence with Eddy Dissipation Rate (EDR) over 0.2 was simulated a couple of hours ahead, but its embedded as small scattered areas within the clouds. The precise location of severe turbulence are still difficult to simulate due to the stochastic nature of turbulence. The seamless blended forecast for significant convection and deep learning model utilising high-pass filtered satellite imageries indicated the growth of convective activity and the presence of convectively induced turbulence in the region. The analysis suggested the importance for having forecasts products showing indication for rapid convective development, which is closely related to convectively induced turbulence or near cloud turbulence. The utilisation of these products within the operations of flights could better safeguard aviation safety.

1 | Introduction

In flight turbulence is one of the well-known hazards that pose serious threats to aviation safety. Turbulence may contribute to injuries or even fatalities for those on board and may also cause structural damage to the aircraft that largely increases the maintenance cost or flight delays when encountering turbulence during the approach phase (Eichenbaum 2003). Therefore, aviation turbulence is not just a concern for safety but also a concern for flight operations and cost. According to the statistics from the United States National Transportation Safety Board (US National Transportation Safety Board 2024), out of the 420 accidents from 2008 to 2022, around 36% (152) of accidents are related to turbulence encounters, ranking first on the list. Over 83% (127) of accidents happened during the enroute phase of flight. This is particularly dangerous as passengers and crews may not expect such turbulence and do not have their seat belt fastened when the flight is cruising enroute. Only around 16% (25) of accidents happened during the climb and approach phases; due to the safety measures implemented and most passengers and crews are seated and securely fastened, many fewer injuries are recorded.

Turbulence or eddies that affect aircraft are called aviation turbulence; it may be formed by different large-scale atmospheric forcing and mechanisms. Aviation turbulence can be classified into different types according to its source (Sharman and Lane 2016):

1. Convectively induced turbulence [CIT] (Lane et al. 2003): It could be in-cloud turbulence, which pilots can visualise the convection via the on-board radar and perform avoidance manipulations. It could also be near-cloud turbulence (NCT) (Lane et al. 2012), which is usually associated with the propagation of gravity waves due to the strong vertical movements within the thermals. NCT usually happens in clear air just outside of the convective clouds and is much more difficult for pilots to avoid as compared with in-cloud turbulence. The lifetime of CIT is relatively short, typically only a few minutes, since it is related to convective cloud features of a much smaller scale.
2. Low level turbulence (LLT): It is usually related to the boundary of two contrasting airmasses or the presence of mechanical obstacles (e.g., buildings). LLT is usually present at the lower boundary layer and mostly affects the take-off and landing phases of aircraft.
3. Mountain wave turbulence (MWT): It is related to gravity waves with larger amplitude in the vicinity of mountains (Doyle et al. 2005; Bramberger et al. 2020). MWT can sometimes be visualised by lenticular clouds or rotor clouds downhill associated with the vortex or eddies when airflow crosses the mountains.
4. Clear air turbulence (CAT) is typically associated with the jet stream or regions with marked horizontal and vertical wind shear, related to Kelvin–Helmholtz instability. These regions can span across hundreds of kilometers horizontally and hundreds of meters vertically. It often appears in cloud-free regions and is not easy for pilots to detect CAT. Due to its 'clear-air' nature, there have been research efforts on consolidating turbulence indices from Numerical Weather Prediction (NWP) models for a reliable turbulence forecast (Ellrod and Knapp 1992; Sharman et al. 2006).
5. Wake vortex: When heavy aircraft flying at low speeds take off or land on the runway, some strong vortex pairs would result from the lift being generated (Hon and Chan 2017). These vortexes usually only affect the runway, and its effect can be reduced by implementing appropriate spacing between subsequent aircraft taking off or landing on the runway.

In the past decade, following the rapid growth of global air traffic, research work has been dedicated to improving the forecast methodologies of the above-mentioned aviation turbulence to safeguard aviation safety for both crews and passengers. However, turbulence predictability varies between the type of aviation turbulence, and the climatology of turbulence varies a lot between regions (Wolff and Sharman 2008; Kim and Chun 2011) depending on the unique topography and climatology of the concerned area. Gisinger et al. (2024) illustrated that the calibrated EDR index forecast from the European Centre for Medium-Range Weather Forecasts (ECMWF) integrated forecasting system (IFS) ensemble prediction system can successfully capture the occurrence of CIT in the vicinity of the convection when convective momentum transport parametrisation was included in the calculation. Different forecast tools need to be developed for the various aviation turbulence types due to the varying length and time scale.

This paper describes the challenges and difficulties in detecting aviation turbulence, especially related to developing thunderstorms, via the investigation of a severe turbulence event with fatalities. The remaining section of the paper is organised as follows: Section 2 describes the severe turbulence event and the utilisation of different remote sensing techniques to understand the basis for the formation of the severe turbulence. Section 3 illustrates related detection and forecast products available in the Hong Kong Observatory (HKO). Section 4 reports on the experiments for simulating the NCT for the event and discusses the insights and challenges. Section 5 presents the discussion and conclusion.

2 | Observational Analysis

Singapore Airlines flight SQ321 departed London at 21:38 UTC on 20 May bound toward southeast for Singapore. The flight encountered severe turbulence when cruising over Myanmar at around 08:00 UTC on 21 May. As there were a number of injured passengers in the cabin, the pilot decided to divert to Suvarnabhumi Airport in Bangkok for medical service. The flight landed in Bangkok at 08:45 UTC on 21 May (Ministry of Transport, 2024). There were multiple injuries and one fatality on board the Boeing 777-300ER aircraft reported by Singapore Airlines. The following analysis attempts to understand the source of this severe turbulence event from a meteorological perspective utilising available remote sensing tools.

2.1 | Turbulence Encountered

To understand the magnitude and location of the turbulence encountered, preliminary analysis was performed on the Automatic Dependent Surveillance—Broadcast (ADS-B) data (granular data) available from https://www.flightradar24.com/, a site with live air traffic data. Note that the analysis relies solely on the frequency available on this set of data. The ADS-B data analysis (Figure 1) showed that SQ321 had experienced a severe turbulence event on 21 May near 16.5 N, 95.2 E at 37,000 ft. above the Irrawaddy Delta, Myanmar. During the flight, the aircraft's altitude did not change much for most of the time before the event, but vertical speed exhibited very significant fluctuations just before and around 07:50 UTC, accompanied by large vertical acceleration.

To understand the severity of the encountered turbulence, the root mean square of vertical acceleration (RMSVA) was evaluated from the ADS-B data. The vertical acceleration was approximated by differentiating vertical rate over a 5 s average gradient, as shown below, where a: vertical acceleration (ms^{-2}), v: vertical rate (ms^{-1}) and t: timestamps (s).

$$a = \frac{\bar{t}\bar{v} - \overline{tv}}{\left(\bar{t}\right)^2 - \overline{t^2}}$$

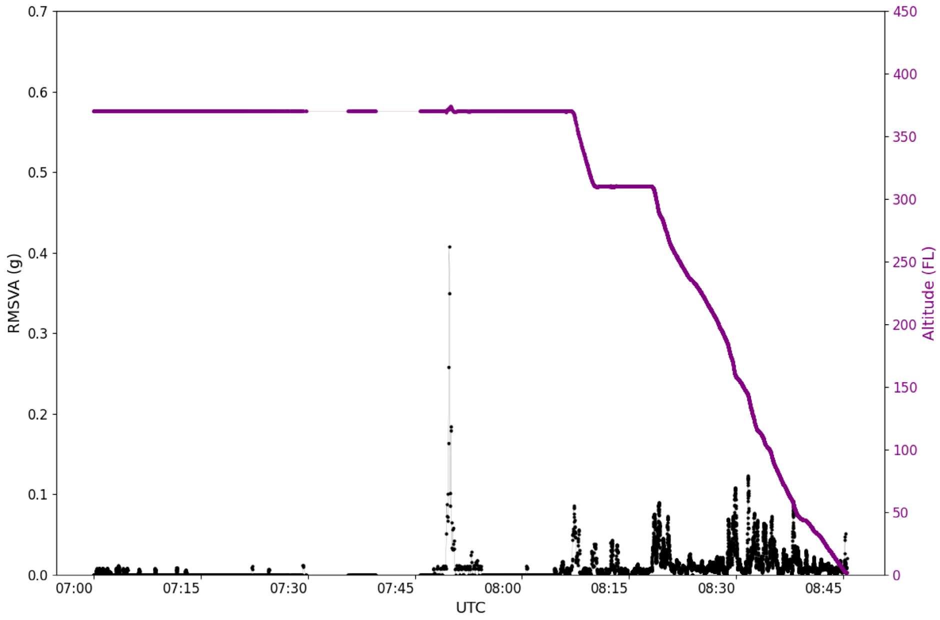

(a)

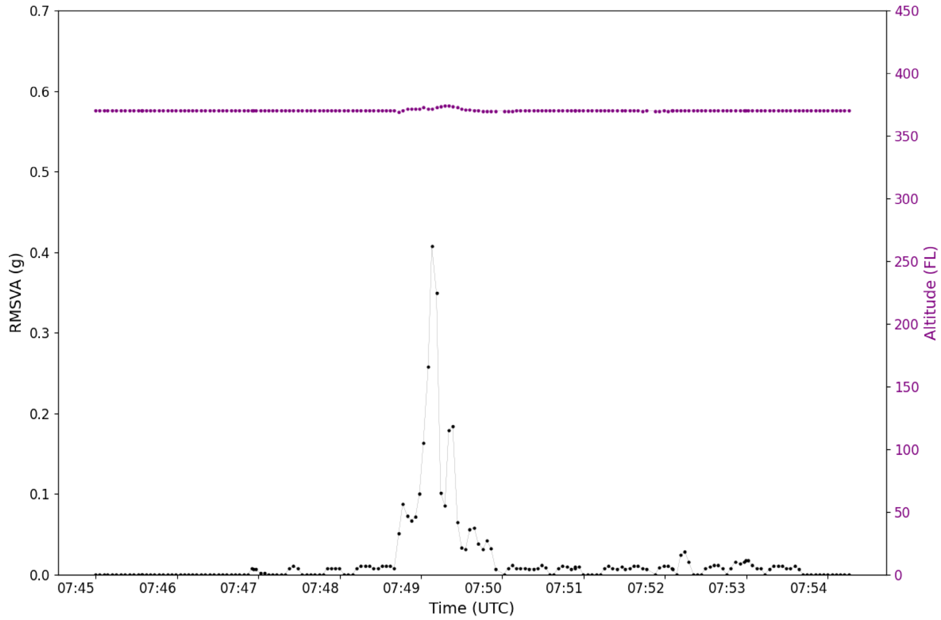

(b)

FIGURE 1 | Time series of RMSVA (black line, left axis) with the right axis (purple line) shows the aircraft altitude (in flight level), (a) shows the time from 0700 to 0845 UTC while (b) shows a zoom in version from 0745 to 0755 UTC.

The RMSVA was then calculated by applying a running 5-s windowed root mean square on a. Noted that the RMSVA is an aircraft-dependent metric and related to the peak load of the aircraft, but probably best correlated with what the pilot or passengers experienced (Bowles and Buck 2009). RMSVA is proportional to Eddy Dissipation Rate (EDR), which is the cube root of the dissipation rate of turbulent kinetic energy (TKE) and a measure of turbulence intensity, via an aircraft response function (Sharman et al. 2014). The derived RMSVA from ADS-B showed that it peaked over 0.4 g (Figure 1) at around 07:50 UTC. The analyzed turbulence encounter time also matched with the preliminary investigation findings (Ministry of Transport, 2024) from Transport Safety Investigation Bureau, Ministry of Singapore. Due to the lack of aircraft response parameters and relevant Mode-S Enhanced Surveillance (EHS) data, this study has no attempt to quantify the EDR from ADS-B which is still an active research area. Nonetheless, the high RMSVA signifies the magnitude of turbulence encountered. Referring to the documented thresholds of RMSVA mentioned in Sharman and Lane, 2016 (shown in Table 1), the observed RMSVA is well above the threshold of 0.3 g denoting severe turbulence. For severe turbulence, crews and passengers are forced violently against seat belts and unsecured ones are tossed within the cabin, leading to the injuries reported. From the online media reports and relevant social media posts, it was observed that the severe turbulence

TABLE 1 | Documented thresholds for RMSVA corresponding to turbulence intensity (Sharman and Lane 2016).

Root mean squared vertical acceleration [RMSVA] (g)	Turbulence intensity
[0.1, 0.2)	Light
[0.2, 0.3)	Moderate
[0.3, 0.6)	Severe
[0.6,∞)	Extreme

occurs when the cabin crew are serving breakfast, leading to more objects to become airborne during the event and the high risk exposed by the cabin crew. Therefore, it is of vital importance to enhance on the detection and forecast of en-route turbulence for better flight route and flight service planning, mitigating the risks on cabin crew and passengers.

2.2 | Remote Sensing Observations

To understand the possible source of this severe turbulence event, remote sensing observational data was investigated and analyzed below.

Cloud top height information for the analyzed time of the turbulence event was shown in Figure 2. The cloud top height was derived from the infrared channel (11.2 μm) of Himawari-9 (Bessho et al. 2016) and Geo-KOMPSAT-2A (Kim et al. 2021) and the vertical profile from the ECMWF model. The satellite images have a spatial resolution of 2 km while the ECMWF model has a resolution of 0.125°. To Himawari-9 and Geokompsat-2A infrared image is first stitched together using a simple linear weighting on the overlapped area. The cloud top pressure was then obtained through linearly interpolating from the model logP-T (log Pressure–Temperature) diagram using the satellite brightness temperature (Leung et al. 2020). From Figure 2, rapid development of convective clouds was evident around the analyzed location of the turbulence event. Cloud top height was well below FL200 at 06:50 UTC, but rapid growth of cloud cluster led to a cloud top height above FL450 at the time of the event. In fact, the cloud cluster near the western coast of Irrawaddy Delta, Myanmar also intensified rapidly and eventually merged with the convective cell over the southeast part of the delta.

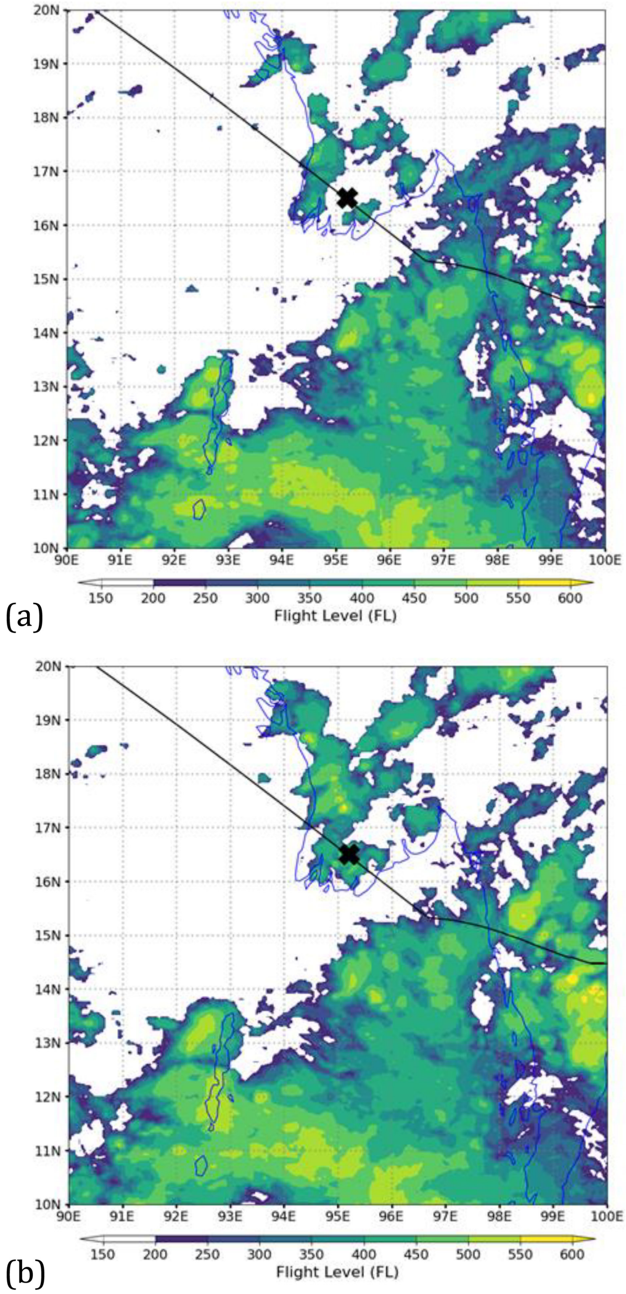

FIGURE 2 | Derived cloud top height information at (a) 06:50 UTC and (b) 07:50 UTC on 21 May 2024. The flight route of SQ321 is plotted as a black line and analyzed location of encountering turbulence is marked as black cross.

To understand the atmospheric circulation for the event, the high resolution wind (HRW) analysis derived from Himawari-9 (Bessho et al. 2016) was utilised. The HRW was derived in-house in HKO for Himawari-9 satellite using the packages available from European Organisation for the Exploitation of Meteorological Satellites (EUMETSAT) Support to Nowcasting and Very Short-Range Forecasting (NWC SAF). The detailed algorithm is illustrated in (AEMET 2021). Figure 3 illustrated the HRW analysis for 150–300 hPa, around FL300-450, which showed the background west-southwesterlies with significant upper level divergence over the western coast of the Irrawaddy Delta, indicating the favourable dynamic factors for rapid development of the cloud cluster. Therefore, the two cloud clusters evident in Figure 2a over the Irrawaddy Delta intensified rapidly and then merged together, which may further enhance wind shear and buoyancy gradients near the cloud tops and instabilities in the vicinity of the development. Global lightning data (Figure 4) from Vaisala (2020) showed abundant lightning activity between the gaps of the two cloud clusters within the past 5 minutes of the suspected event time. The majority of them are cloud-to-ground lightning, which demonstrated a high content of ice particles that favours the initiation of electrical activity (Mattos and Luiz A.T. Machado, Mattos and Machado 2011) and the presence of strong vertical movement.

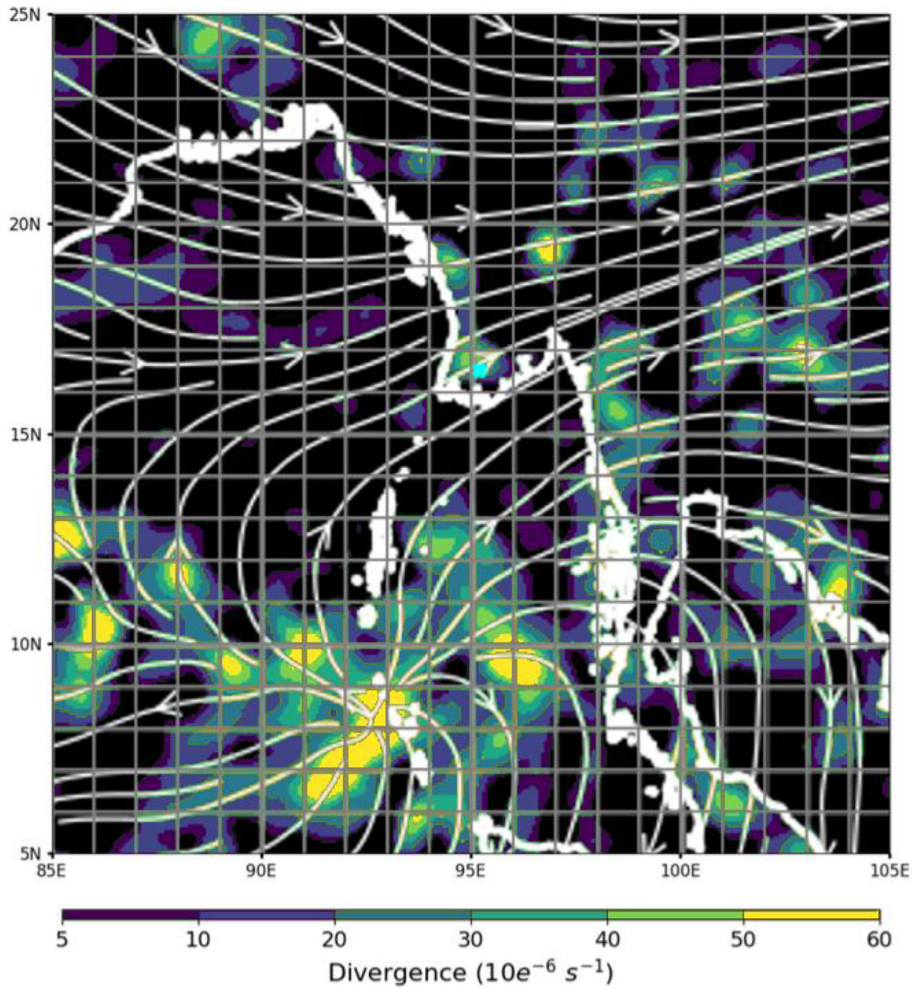

FIGURE 3 | The wind streamlines analysis (isolines) and the divergence field (contour) from Himawari-9 satellite (based on High Resolution Winds from NWCSAF) for 150–300 hPa at 06Z on 21 May 2024.

Based on the above observations, the severe turbulence encountered by SQ321 was likely to be related to convectively induced turbulence and could be a mixture of in-cloud CIT and NCT. This aligns with the presence of an area of developing convective activity mentioned in the preliminary investigation findings (Ministry of Transport, 2024).

3 | MPAS Simulation

3.1 | Data and Methodology

To understand the turbulence event and its predictability, a simulation utilising the Model for Prediction Across Scales (MPAS) model was performed. MPAS applied unstructured Voronoi meshes and C-grid discretisation (Skamarock et al. 2012). A regional refined global mesh is designed for this case. This mesh has a 3-km resolution, which is a convection-permitting mesh, near the location of the turbulence and a 60-km resolution in the background (Figure S1 in Supporting Information). Therefore, MPAS can simulate large-scale circulation and small-scale convection under limited computational resources. The model has 55 vertical levels and the top is at 30 km. The interval of vertical levels is about 500–700 m. The convection parameterisation was turned off since the resolution utilised in the simulation was convection-permitting (Chen et al. 2024). The Tompson microphysics scheme, MYNN planetary boundary layer scheme and Noah land surface scheme were used in the simulation. These combinations are commonly applied in other research using the MPAS model (Landu et al. 2014; Hagos et al. 2015). The experiment was initialised using ECMWF Reanalysis v5 (ERA5) data with a 0.25° resolution and the lead time is 4 h to obtain a balance for predictability and forecast results.

Simulated data from the MPAS model was then interpolated to a rectangular grid for further applications. Wind field of the experiments are utilised to calculate EDR by using the explicit filtering and reconstruction in turbulence parameterisation (Chow et al. 2005). In this method, Subfilter scales can be divided into resolvable subfilter scales (RSFS) and subgrid scales (SGS). We only calculated RSFS part since it accounts for most of the energy (Chen et al. 2024). We did zero-order reconstruction in this study as including more terms may occasionally generate negative TKE which is unrealistic. So we have $\widetilde{\overline{u_i^*}} = \widetilde{u}_i$. Here u is the velocity along different directions, overline represents the filter, the tilde represents discretisation, $\widetilde{u}_i$ is the variable from the model.

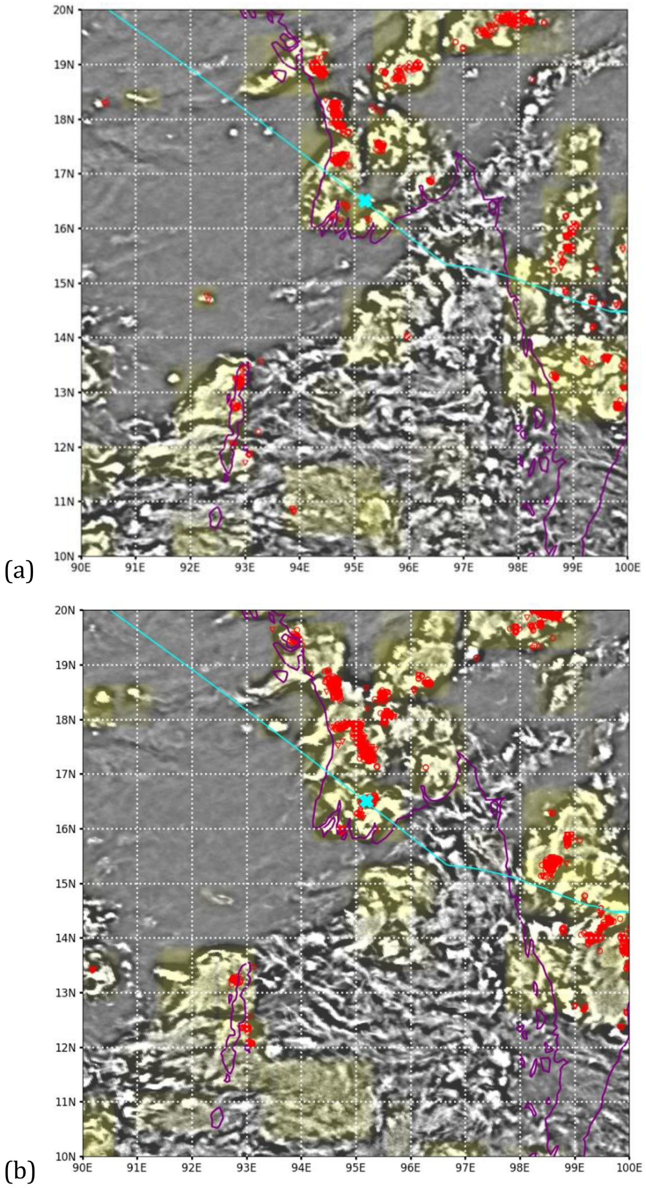

FIGURE 4 | Locations of lightning detected for (a) 06:45–06:50 UTC and (b) 07:45–07:50 UTC indicated as red circle (cloud-to-cloud lightning) and red triangle (cloud-to-ground lightning). Lightning was overlaid on the high-pass filtered Himawari-9 satellite image at (a) 06:50 UTC and (b) 07:50 UTC on 21 May. Area highlighted in yellow indicates CIT identified by the auto-detection model. The flight route of SQ321 is plotted as a cyan line and analysed location of encountering turbulence is marked as cyan cross.

The RSFS TKE is calculated by

$$\mathrm{TKE} = \frac{1}{2}\left(\overline{\widetilde{u_i^*}\widetilde{u_i^*}} - \overline{\widetilde{u}_i^*}\ \ \overline{\widetilde{u}_i^*}\right)$$

Assuming the scale of turbulence is included in the inertial subrange, the EDR can be expressed as follows (Schumann 1991):

$$\varepsilon^{1/3} = \left(\mathrm{TKE}^{3/2}/L\right)^{1/3}$$

Before applying the equations, MPAS data were interpolated to a 0.04°*0.04° rectangular grid using the bilinear method from the

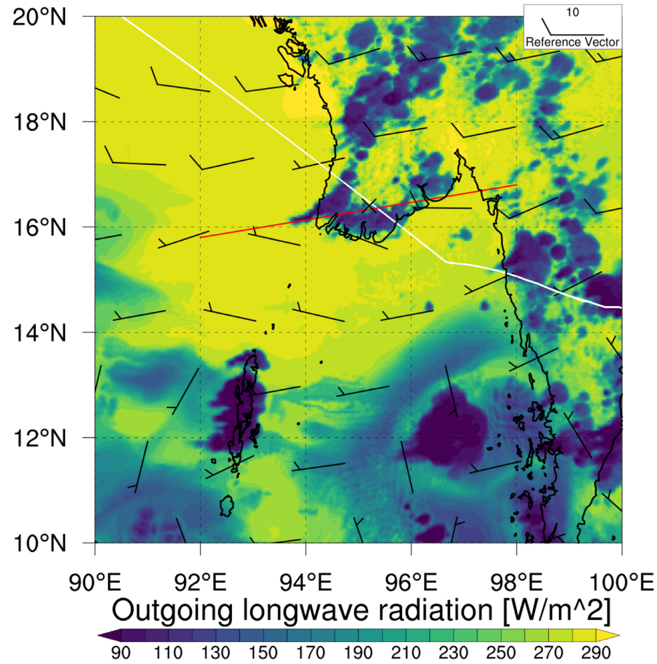

FIGURE 5 | Outgoing longwave radiation and wind field at 11200 m on MPAS model at 0750UTC on 21 May. The flight route of SQ321 is plotted as a white line and analysed location of encountering turbulence is marked as black cross. The red line represents the cross-section in Figure 6.

Earth System Modeling Framework library (Brown et al. 2012). Here we used Butterworth filter horizontally and 1-2-1 filter (Chow et al. 2005) vertically to calculate the scale of the turbulence, $L = (\lambda \Delta x \Delta y \Delta z)^{1/3}$, Δx, Δy and Δz are grid spacings, the λ can be derived based on the cutoff wavelength of the filter. It was set as 2 in this study (Chen et al. 2024). This method is commonly employed for regridding MPAS hexagon mesh data (Xu et al. 2021). Consequently, for the region proximate to Southeast Asia, Δx and Δy are approximately 4.5 km, while Δz, representing the grid spacing in the middle troposphere, is 500 m.

3.2 | Results

Figure 5 showed the Outgoing Longwave Radiation (OLR) in MPAS model at 0750UTC on 21 May. It was observed that the simulated convective clouds are mostly along the coast of Irrawaddy Delta, Myanmar. This was consistent with the observed convective clouds on satellite images and reflects the correlation between turbulent activities and convective developments in this case. A vertical cross section plot along the prevailing wind direction across the location of the turbulence event was shown in Figure 6. Strong vertical updrafts were observed in the simulation near the location of turbulence. Figure 6 also showed the presence of atmospheric gravity waves (AGWs) with a wave length of approximately 10 km at the downwind side to the west of the turbulence location. These AGWs demonstrate that the perturbed wind field in the vicinity of the deep convection and associated turbulence would be more likely to occur in this situation. Overturning of potential temperature was observed near the AGWs which matched with the waves observed on the high pass filtered satellite image in Figure 4 (refer to

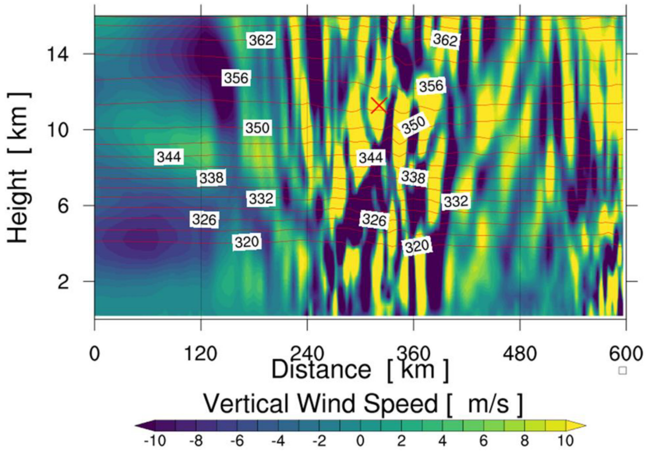

FIGURE 6 | A vertical cross section (red line in Figure 5) on the vertical wind speed of MPAS model overlaid with potential temperature from 15.5°N, 92°E to 16.5°N, 98°E at 0750 UTC on 21 May. The analysed location of encountering turbulence is marked as a red cross. The X-axis represents the number of grid points, with a grid point size of 0.04°.

Section 4.1 for details of the satellite image). This also indicates atmospheric instability and turbulent flow mixing in the vicinity of the event.

Chen et al. (2024) indicated that the sensitivity of the selection of the vertical cross section should be examined. By adjusting the latitude of the profile, different results were obtained and relevant figures was shown in Figure 7a,b. All figures show the presence of gravity waves at a height below the notation 'X', the location of the turbulence, indicating a similar pattern in the atmospheric environment around the region. Therefore, although predicting the precise location and time of a deep convection remains challenging, MPAS still provides meaningful turbulence predictions and hints on the physical mechanisms for potential high-risk areas.

Figure 8 showed the simulated EDR values at 37,000 ft (11,200 m), the height at which turbulence was encountered. It was observed that EDR values showed a similar distribution as the OLR (i.e., convective cloud) along the coast of the delta region. Moderate turbulence, with EDR values > 0.2 (shown as yellowish) is embedded as small scattered areas within the clouds, indicative of small-scale deep convection. The turbulence encountered in this event is possibly due to the rapid development of deep convection, triggering gravity waves and breaking of waves, forming turbulent eddies. This physical scenario has been described in Lane et al. (2003) by using high-resolution models in the order of tens of meters.

In fact, for regions further north, there exists stronger turbulence with EDR > 0.3. Figure 7c showed the vertical profile further north in proximity to the high EDR values. The vertical profile is similar to Figures 6 and 7a,b, but the breaking of gravity waves induced by convection is more pronounced in Figure 7c, resulting in higher EDR intensity. As shown in Figure 5, the wind direction over Myanmar is dominated mainly by westerlies, while the locations of convection and stronger turbulence are nearly perpendicular to the background wind. Additionally, the spatial distribution of convection aligns with the mountainous terrain of Myanmar, suggesting that topography also acts a significant role in shaping the weather patterns in the region.

We analyzed the horizontal distribution of EDR at 10-min intervals during the hour preceding the turbulence event (Figure S2 in Supporting Information). Under stable background conditions—specifically, persistent westerlies with minimal variations in wind speed and direction in this case—both the spatial locations and intensity of turbulence showed negligible temporal changes. This stability allowed turbulence structures (e.g., localised 'point-like' clusters) to remain consistent over time. These findings demonstrate that turbulence forecasts retain practical utility even with slight timing mismatches between prediction and aircraft operations. When background winds are stable, the horizontal distribution and intensity patterns evolve slowly enough to provide reliable guidance, despite potential discrepancies in exact event timing.

The MPAS model utilised in this study in convection-permitting scale can capture turbulence produced by a similar mechanism. The simulation showed high-resolution MPAS model can simulate the convective clouds along the coast and have some indication of moderate turbulence around the turbulence event a couple of hours ahead of the event.

3.3 | Limitations of Simulation

Although the simulation has some indication of moderate turbulence around the event location, indication of severe turbulence (EDR values over 0.45) was lacking. This could be due to the utilisation of coarse resolution reanalysis data (ERA5 with 0.25° resolution) which failed to give indications of small scale deep convective waves related to the deep convection development. The resolution itself prevents EDR from being calculated to a larger value, because the physical quantities are still smoothed as average values within the grid, and the measurement scale of the aircraft's sensors is inevitably much smaller than the 3 km grid. In addition, CIT from fast-growing deep convection is always very transient. The position of the turbulence areas and the magnitude of the EDR may not be very accurate. Predicting small scale convective turbulence presented in this case may require more computational resources to improve on the mesh and time resolution. This may contribute to a more precise EDR value (Barber et al. 2017). Rapidly updating data assimilation may also assist in capturing the growth of the convective cells, giving finer details for the model to simulate and forecast. Another approach is to use ERA5 ensemble initial conditions for ensemble forecasting of small-scale disturbances.

4 | Detection and Forecast Products

International Civil Aviation Organisation Annex 3 specified the Meteorological Watch Offices shall issue Significant Weather Information (SIGMET) concerning the occurrence or expected occurrence of specified en-route weather and other phenomena in the atmosphere that may affect the safety of aircraft operations within the designated airspace. One of the hazardous weather phenomena is thunderstorms, which cover the associated hazards like turbulence and icing. Besides SIGMET, which

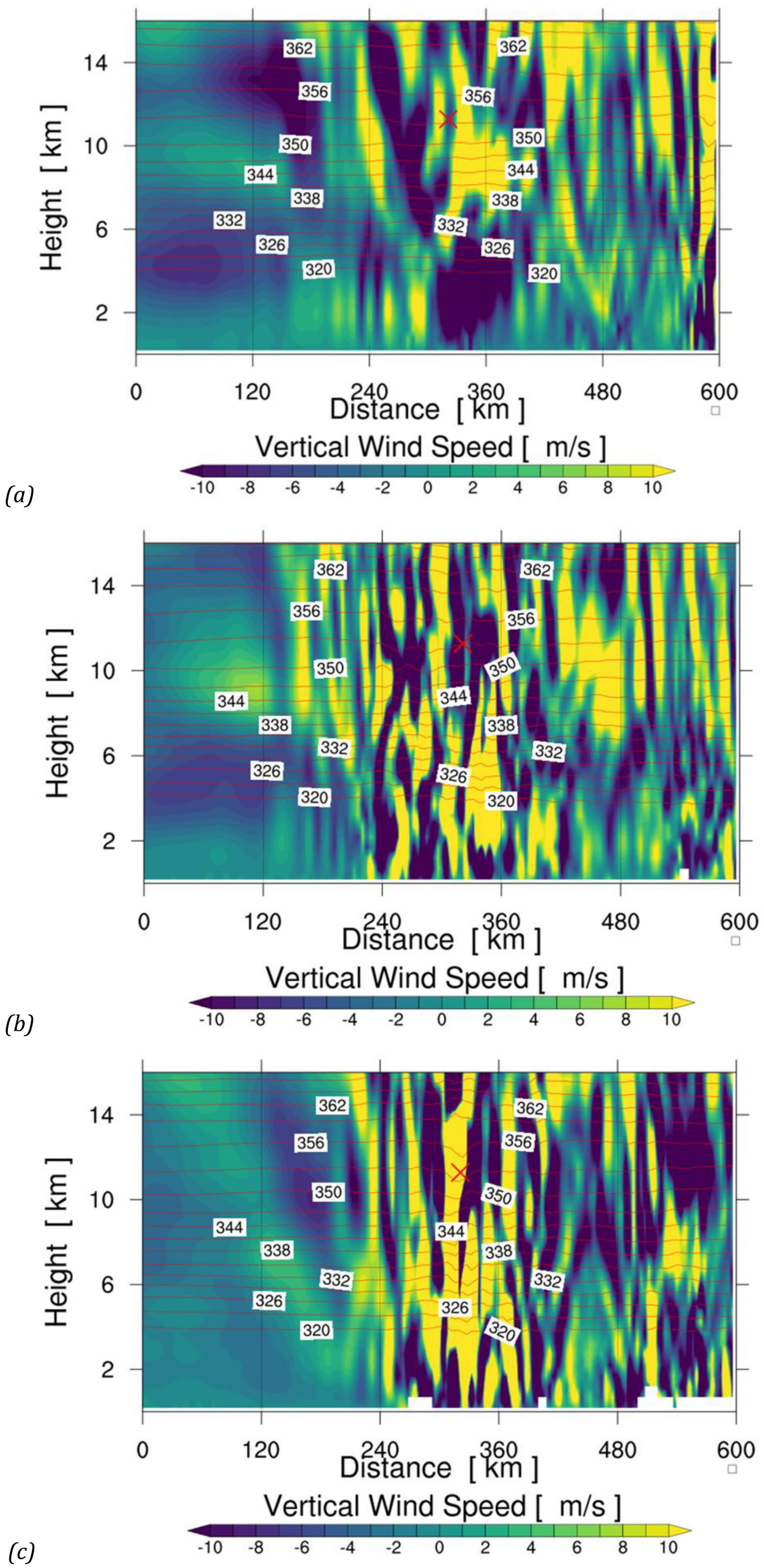

FIGURE 7 | A vertical cross section on the vertical wind speed of MPAS model overlaid with potential temperature (a) from 15.2°N, 92°E to 16.2°N, 98°E (0.3 southwards compared with Figure 6) and (b) from 15.8°N, 92°E to 16.8°N, 98°E (0.3° northwards compared with Figure 6) and (c) 17.2°N, 92°E to 18.2°N, 98°E (1.7° northwards compared with Figure 6) at 0750 UTC on 21 May. The analysed location of encountering turbulence is marked as a red cross. The X-axis represents the number of grid points, with a grid point size of 0.04°.

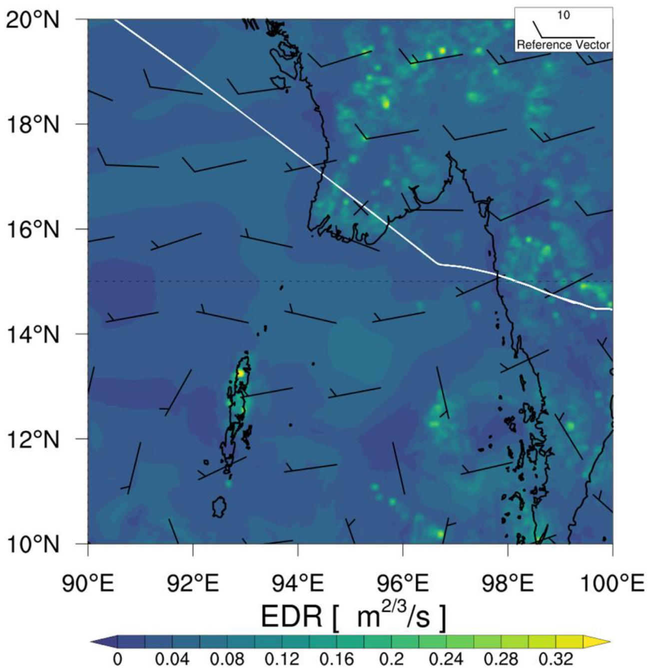

FIGURE 8 | Simulated EDR values and wind field at 11200 m of MPAS model at 0750 UTC on 21 May. The flight route of SQ321 is plotted as a white line and analysed location of encountering turbulence is marked as black cross.

is more general and available in real time and in the nowcasting timescale of 0–4 h ahead, we investigated the below two products developed by HKO that are more specific on CIT/NCT and a blended forecast with longer forecast hours.

4.1 | Deep Learning Model for Detection of Turbulence From AGW Features

Some aviation turbulence is closely related to AGW, which can sometimes be visualised from satellite images. HKO developed an in-house deep learning model for the detection of AGW from high-pass filtered Himawari-9 satellite images (Chan et al. 2022). The Gaussian high-pass filtering (Wimmers et al. 2018) was first applied to the Himawari-9 water vapour channel images (6.2 μm) for highlighting AGW, displaying only the variations from −1 to +1 K of brightness temperature from the local average. A greyscale image was utilised to show the full range of gravity wave features. The filter applied is shown below with σ as the width parameter and c is a constant that allows the weights to sum to unity, x and y is the distance from the local average position (i.e., the spatial extents in the x, y dimensions for the filter). The width parameter σ was set as x and the local region was calculated for x. was The high pass filter $HP(\sigma)$ allows the user to examine the variations in the relative image value, but not the absolute image value, which can isolate the signature of gravity waves. The calculation is illustrated below, with I_{hp} is the high pass filtered image and I is the initial image.

$$I_{\mathrm{hp}} = \mathrm{HP}(\sigma) * I$$

$$\mathrm{HP}(\sigma) = 1 - \frac{c}{\sigma\sqrt{2\pi}} \sum_{x,y} e^{-\frac{x^2+y^2}{2\sigma^2}}$$

Aiming to automatically identify the AGW and associated turbulence, the processed high-pass filtered satellite images are trained with actual turbulence observations from pilot reports. The deep learning model was built utilising the processed satellite images collected over T ± 30 min from the observation time of pilot reports. Over 750 pilot reports from January 2018 to June 2021 were collected for the training and validation. The model utilised the Faster Region-based Convolutional Neural Network (Faster-RCNN) with a train-test ratio of 80:20. The developed product can automatically classify features related to AGWs on satellite imageries as severe turbulence, significant severe turbulence and convection-induced turbulence as highlighted regions. The AGW features can also be analyzed with the highlighted regions overlaid onto the high-pass filtered imageries. Figure 4 showed the deep learning detection model successfully highlighted the region with convection-induced turbulence (shaded in yellow) around the location of the turbulence event. AGW features highlighted from the high-pass filtered indicated the deepening of cloud edges and the gradual build-up of waves in the vicinity of the turbulence event.

Currently, this satellite product has been produced routinely for operational use. However, such satellite product would take time to produce in real time due to the observation time required for satellite imageries and subsequent transmission and processing time. Predictability from this product would rely on any precursor and development signals shown on the satellite image. In this case, the high pass filtered images at 06:50 UTC (Figure 4a) showed signs of gravity waves in the vicinity highlighted with black contours. The deep learning detection model (areas highlighted in yellow) already covered the incident location at 06:50 UTC in the vicinity of the edge of the gravity waves, giving early hints of CIT in the area. At 07:50 UTC (Figure 4b), gravity waves were evident over the whole of Irrawaddy Delta and the CIT signal (areas highlighted in yellow) remains. This satellite product would be useful as nowcasting for developing convective clouds that induce CIT. Nonetheless, as the high pass filtered image is based on the latest satellite image and trained for detection purposes, it would only be useful in the nowcasting range within 1 hour.

4.2 | Seamless Blended Significant Convection Forecast

To support gate-to-gate operations and trajectory-based operations for the next generation of aviation weather service, a study to bridge nowcast and NWP model was formulated. A seamless significant convection forecast system (Cheung et al. 2024) is developed through the blending of outputs from satellite nowcasting system and NWP model precipitation outputs. The satellite nowcasting system is based on the extrapolation of the satellite identified convection based on its past movement, it has a prediction up to T + 8. The NWP model utilised here is the ECMWF IFS High Resolution forecast (HRES) with predictions up to 10 days. The NWP model precipitation intensity forecast was first corrected via frequency matching against the ground truth T + 0 of satellite nowcast. Weighted blending scheme was then applied to blend the satellite nowcast and NWP model outputs at each forecast hour from T + 0 to T + 8. A salient cross dissolve (SalCD) blending

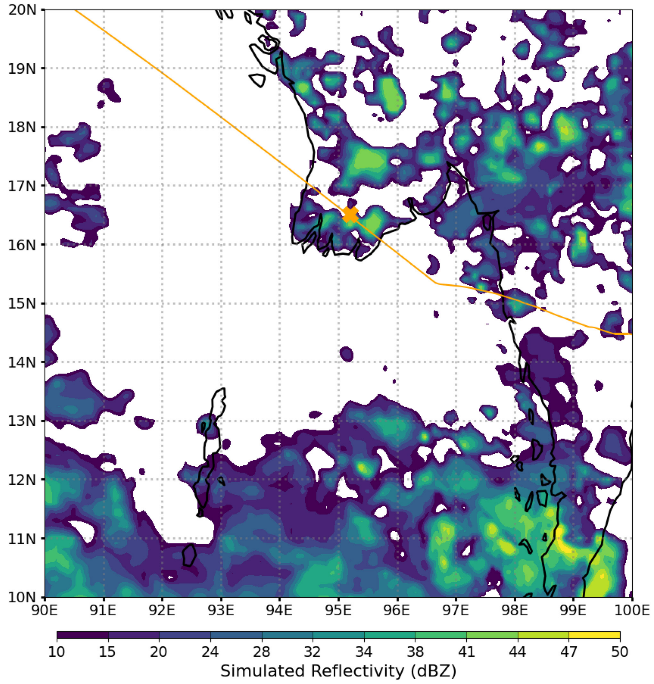

FIGURE 9 | Seamless significant convection forecast valid at 08Z on 21 May for model run initialised at 00Z on 21 May. The flight route of SQ321 is plotted as an orange line and the analysed location of encountering turbulence is marked as an orange cross.

(Hwang et al. 2015) was utilised in the study and found its performance was superior to other blending schemes (e.g., simple linear blending). SalCD considers the normalised intensities of the NWP model and satellite nowcast. The idea is to preserve strong pixels by modifying w_{nwp} as a function of reflectivity Z_{nwp} and Z_{nowcast}. The SalCD-blended reflectivity Z_{salcd} is described by the following equations

$$Z_{salcd} = ws_{nwp} Z_{\text{nowcast}} + \left(1 - ws_{nwp}\right) Z_{\text{nowcast}}$$

$$ws_{nwp} = \frac{1}{2}\left[\frac{w_{nwp} I}{\left(w_{nwp} I\right) + \left(1 - w_{nwp}\right)(1 - I)} + \frac{\sqrt{w_{nwp}{}^2 + I^2}}{\sqrt{w_{nwp}{}^2 + I^2} + \sqrt{\left(1 - w_{nwp}\right)^2 + (1 - I)^2}}\right]$$

$$I = F\left(N_{nwp} - N_{\text{nowcast}}\right)$$

where salience I refers to the cumulative distribution function of the difference in normalised NWP model reflectivity N_{nwp} and normalised satellite nowcast N_{nowcast}. The relation of NWP model weight for SalCD blending ws_{nwp}, NWP model weight w_{nwp} and salience I is shown in Figure S3 in Supporting Information. Preserving strong intensity precipitation forecasts is beneficial to the blended significant convection forecast which targeted aviation users. Aviation users, in contrary to the general public, would be most concern about intense convection that may affect their operations rather than light precipitation condition. The weightings for satellite nowcast and NWP model outputs in the blended forecast are based on past year performance (usually more satellite nowcast from T + 0 to T + 3 while the NWP model outputs are getting more important from T + 4 onwards).

Initialised at 00Z on 21 May, the T + 8 blended forecast (valid at 08Z on 21 May) can successfully capture the development of intense convection (Figure 9) with simulated reflectivity over 41 dBZ around the location of the event. The blended forecast for significant convection has been running routinely in HKO since 2023 and has supplemented in real-time the air traffic flow management of the Hong Kong Civil Aviation Department. The blended forecast is superior as compared with the extrapolation of satellite nowcast as it assembles the NWP forecast output for the growth and decay of convection. In the context of CIT/NCT, Barber and Mullendore (2020) indicated that the decrease of static stability and increase of vertical wind shear near developing convection provided more favourable conditions for turbulence production. The successful capture of the growth of convection for the blended forecast may then indicate the increased risks of turbulence in its vicinity.

This seamless blended forecast would be available a few hours (up to 8 h) before the turbulence event happened, which could potentially benefit the flight operations by suggesting hints of convective hazard along the flight route. It would be beneficial to extend the usage of the blended forecast to other users in the aviation community.

5 | Discussion and Conclusion

This paper presented the analysis of a severe turbulence event aloft Myanmar on 21 May 2024. Analysis from available ADS-B data indicated a severe turbulence event occurred with large vertical acceleration, which contributed to the injuries and fatalities on board if they were not properly secured by seat belt at the time of turbulence occurrence. Satellite, cloud tops and lightning data analysis showed the turbulence is most probably CIT or NCT in relation to the breaking waves of rapidly developing convective cells downwind. Deep learning model on high-pass filtered imageries gives indication of these gravity waves.

Simulation model at convective permitting resolution showed that due to the small-scale nature of this convection, it is still difficult to forecast precise EDR values that indicate severe turbulence at the precise location and height. But it still indicated these perturbations and related turbulence can be captured in the model; at least the turbulence active areas located over southern Myanmar were successfully predicted. The skill of the simulation could be better if ensemble experiments were applied to capture the randomness. Nonetheless, blended forecast product utilising both satellite nowcast and NWP model rainfall predictions can potentially indicate early alert to pilots several hours ago on the development of significant convective cells. It is hoped that the development of these detections and forecast products could safeguard aviation safety and provide early awareness for similar events like this and prevent injuries from happening again.

Author Contributions

Christy Yan Yu Leung: conceptualization, methodology, formal analysis, visualization, resources, writing – original draft. **Haoming Chen:** methodology, formal analysis, visualization, writing – original draft. **Xiaoming Shi:** project administration, funding acquisition, methodology, writing – review and editing. **Ping Cheung:** project administration, funding acquisition, writing – review and editing. **Pak Wai Chan:** conceptualization, formal analysis, writing – review and editing.

Acknowledgements

The project is part of the Aviation Research and Development Project Phase 2 (AvRDP2), supported by the World Meteorological Organisation. X.S. and H.C. also thank the Research Grant Council of Hong Kong SAR, China (HKUST-16301322) for its support. The authors thank HKUST Fok Ying Tung Research Institute and the National Supercomputing Center in Guangzhou Nansha subcenter for providing high-performance computational resources. Also, the authors thank the development teams of Hong Kong Observatory for the deep learning AGW model and blended forecast for supplementing this paper with the forecast products.

Conflicts of Interest

The authors declare no conflicts of interest.

Data Availability Statement

The ADS-B data that support the findings of the study are publicly available at https://www.flightradar24.com/blog/wp-content/uploads/2024/05/Flightradar24_SQ321_Granular_Data.csv. Other observations and forecast data are available upon reasonable request to the Hong Kong Observatory.

References

AEMET. 2021. "Algorithm Theoretical Basis Docuement for the Wind product Processor of the NWC/GEO. NWP/CDOP3/GEO/AEMET/SCI/ATBD/Wind." https://www.nwcsaf.org/aemetRest/downloadAttachment/6474.

Barber, K. A., and G. L. Mullendore. 2020. "The Importance of Convective Stage on out-Of-Cloud Convectively Induced Turbulence From High-Resolution Simulations." *Monthly Weather Review* 148, no. 11: 4587–4605. https://doi.org/10.1175/MWR-D-20-0065.1.

Barber, K. A., G. L. Mullendore, and M. J. Alexander. 2017. "Out-Of-Cloud Convective Turbulence: Estimation Method and Impacts of Model Resolution." *Journal of Applied Meteorology and Climatology* 57, no. 1: 121–136. https://doi.org/10.1175/JAMC-D-17-0174.1.

Bessho, K., K. Date, M. Hayashi, et al. 2016. "An Introduction to Himawari-8/9—Japan's New-Generation Geostationary Meteorological Satellites." *Journal of the Meteorological Society of Japan. Ser. II* 94, no. 2: 151–183.

Bowles, R. L., and B. K. Buck. 2009. "A Methodology for Determining Statistical Performance Compliance for Airborne Doppler Radar With Forward-Looking Turbulence Detection Capability. NASA Contractor Report. NASA/CR-2009-215769." http://ntrs.nasa.gov/archive/nasa/casi.ntrs.nasa.gov/20090025483.pdf.

Bramberger, M., A. Dörnbrack, H. Wilms, F. Ewald, and R. Sharman. 2020. "Mountain-Wave Turbulence Encounter of the Research Aircraft HALO Above Iceland." *Journal of Applied Meteorology and Climatology* 59, no. 3: 567–588. https://doi.org/10.1175/jamc-d-19-0079.1.

Brown, D., R. Brownrigg, M. Haley, and W. Huang. 2012. "NCAR Command Language (NCL). UCAR/NCAR—Computational and Information Systems Laboratory (CISL)."

Chan, Y. W., W. H. Tang, and K. C. Cheung. 2022. "Operational Application of Deep Learning Model for Auto-Detection of Atmospheric Gravity Waves Over the Asia-Pacific region. 12th Asia-Oceania Meteorological Satellite Users' Conference (AOMSUC-12), Online, 11–18 November 2022." https://www.data.jma.go.jp/mscweb/en/aomsuc12/presentation/S42_15.pdf.

Chen, H., Shi, X., Nie, X., Wang, Y., Leung, C. Y. Y., Cheung, P., & Chan, P. W. 2024. "Tropical Aviation Turbulence Induced by the Interaction Between a Jet Stream and Deep Convection." *Journal of Geophysical Research: Atmospheres* 129, no. 18. https://doi.org/10.1029/2024jd040763.

Cheung, O.-P., Y.-L. Ng, C. Y.-Y. Leung, and M.-H. Kok. 2024. "Seamless Significant Convection Forecast for Aviation, EMS Annual Meeting 2024, Barcelona, Spain, 1–6 Sep 2024, EMS2024-632." https://doi.org/10.5194/ems2024-632.

Chow, F. K., R. L. Street, M. Xue, and J. H. Ferziger. 2005. "Expicit Filtering and Reconstruction Turbulence Modeling for Large-Eddy Simulation of Neutral Boundary Layer Flow." *Journal of the Atmospheric Sciences* 62, no. 7: 2058–2077. https://doi.org/10.1175/JAS3456.1.

Doyle, J. D., M. A. Shapiro, Q. Jiang, and D. L. Bartels. 2005. "Large-Amplitude Mountain Wave Breaking Over Greenland." *Journal of the Atmospheric Sciences* 62, no. 9: 3106–3126. https://doi.org/10.1175/jas3528.1.

Eichenbaum, H. 2003. "Historical Overview of Turbulence Accidents and Case Study Analysis. MCR Federal Inc. Rep. Br-M021/080–1, 82."

Ellrod, G. P., and D. E. Knapp. 1992. "An Objective Clear-Air Turbulence Forecasting Technique: Verification and Operational Use." *Weather and Forecasting* 7, no. 1: 150–165. https://doi.org/10.1175/1520-0434(1992)007%3C0150:aocatf%3E2.0.co;2.

Gisinger, S., M. Bramberger, A. Dörnbrack, and P. Bechtold. 2024. "Severe Convectively Induced Turbulence Hitting a Passenger Aircraft and Its Forecast by the ECMWF IFS Model." *Geophysical Research Letters* 51, no. 23. https://doi.org/10.1029/2024GL113037.

Hagos, S., L. R. Leung, Q. Yang, C. Zhao, and J. Lu. 2015. "Resolution and Dynamical Core Dependence of Atmospheric River Frequency in Global Model Simulations." *Journal of Climate* 28, no. 7: 2764–2776. https://doi.org/10.1175/JCLI-D-14-00567.1.

Hon, K. K., and P. W. Chan. 2017. "Aircraft Wake Vortex Observations in Hong Kong." *Journal of Radars* 6, no. 6: 709–718. https://doi.org/10.12000/jr17072.

Hwang, Y., A. J. Clark, V. Lakshmanan, and S. E. Koch. 2015. "Improved Nowcasts by Blending Extrapolation and Model Forecasts." *Weather and Forecasting* 30, no. 5: 1201–1217. https://doi.org/10.1175/waf-d-15-0057.1.

Kim, D., M. Gu, T. H. Oh, E. K. Kim, and H. J. Yang. 2021. "Introduction of the Advanced Meteorological Imager of Geo-Kompsat-2a: In-Orbit Tests and Performance Validation." *Remote Sensing* 13, no. 7: 1303. https://doi.org/10.3390/rs13071303.

Kim, J.-H., and H.-Y. Chun. 2011. "Statistics and Possible Sources of Aviation Turbulence Over South Korea." *Journal of Applied Meteorology and Climatology* 50, no. 2: 311–324. https://doi.org/10.1175/2010jamc2492.1.

Landu, K., L. R. Leung, S. Hagos, et al. 2014. "The Dependence of ITCZ Structure on Model Resolution and Dynamical Core in Aquaplanet Simulations." *Journal of Climate* 27, no. 6: 2375–2385. https://doi.org/10.1175/JCLI-D-13-00269.1681.

Lane, T. P., R. D. Sharman, T. L. Clark, and H. M. Hsu. 2003. "An Investigation of Turbulence Generation Mechanisms Above Deep Convection." *Journal of the Atmospheric Sciences* 60, no. 10: 1297–1321. https://doi.org/10.1175/15200469(2003)60<1297:AIOTGM>2.0.CO;2.

Lane, T. P., R. D. Sharman, S. B. Trier, R. G. Fovell, and J. K. Williams. 2012. "Recent Advances in the Understanding of Near-Cloud

Turbulence." *Bulletin of the American Meteorological Society* 93, no. 4: 499–515. https://doi.org/10.1175/bams-d-11-00062.1.

Leung, Y. Y. C., H. Tam, W. Chan, and H. Fok. 2020. "Development of Satellite-Based Cloud Top Height and Convection Nowcasting Products in Support of SIGMET Coordination in APAC Region. 20th Conference on Aviation, Range and Aerospace Meteorology, Boston, United States of America, 16 January 2020." https://ams.confex.com/ams/2020Annual/mediafile/Manuscript/Paper362417/12_2_extended_abstract_final.pdf.

Mattos, E. V., and L. A. T. Machado. 2011. "Cloud-To-Ground Lightning and Mesoscale Convective Systems." *Atmospheric Research* 99, no. 3–4: 377–390. https://doi.org/10.1016/j.atmosres.2010.11.007.

Schumann, U. 1991. "Subgrid Length-Scales for Large-Eddy Simulation of Stratified Turbulence." *Theoretical and Computational Fluid Dynamics* 2, no. 5: 279–290. https://doi.org/10.1007/BF00271468.

Sharman, R., L. Cornman, G. Meymaris, J. E. Pearson, and T. C. Farrar. 2014. "Description and Derived Climatologies of Automated in Situ Eddy-Dissipation-Rate Reports of Atmospheric Turbulence." *Journal of Applied Meteorology and Climatology* 53, no. 6: 1416–1432. https://doi.org/10.1175/jamc-d-13-0329.1.

Sharman, R., and T. Lane. 2016. *Aviation Turbulence: Processes, Detection, Prediction*. Springer International Publishing. https://doi.org/10.1007/978-3-319-23630-8

Sharman, R., C. Tebaldi, G. Wiener, and J. Wolff. 2006. "An Integrated Approach to Mid- and Upper-Level Turbulence Forecasting." *Weather and Forecasting* 21, no. 3: 268–287. https://doi.org/10.1175/waf924.1.

Skamarock, W. C., J. B. Klemp, M. G., Duda, L. D., Fowler, S. -H., Park and T. D. Ringler. 2012. "A Multiscale Nonhydrostatic Atmospheric Model Using Centroidal Voronoi Tesselations and C-Grid Staggering." *Monthly Weather Review* 140, no. 9: 3090–3105. https://doi.org/10.1175/mwr-d-11-00215.1.

Ministry of Transport. "Transport Safety Investigation Bureau Preliminary Investigation Findings of Incident Involving sq321." 2024. [online] https://www.mot.gov.sg/news/Details/transport-safety-investigation-bureau-preliminary-investigation-findings-of-incident-involving-sq321.

US National Transportation Safety Board. 2024. "US Civil Aviation Accident Dashboard: 2008–2022." [online] https://www.ntsb.gov/safety/StatisticalReviews/Pages/CivilAviationDashboard.aspx.

Vaisala. 2020. "Global Lightning Detection Network (GLD360) [Online]." https://www.vaisala.com/en/products/systems/lightning/gld360.

Wimmers, A., S. Griffin, J. Gerth, S. Bachmeier, and S. Lindstrom. 2018. "Observations of Gravity Waves With High-Pass Filtering in the New Generation of Geostationary Imagers and Their Relation to Aircraft Turbulence." *Weather and Forecasting* 33, no. 1: 139–144. https://doi.org/10.1175/WAF-D-17-0080.1.

Wolff, J. K., and R. D. Sharman. 2008. "Climatology of Upper-Level Turbulence Over the Contiguous United States." *Journal of Applied Meteorology and Climatology* 47, no. 8: 2198–2214. https://doi.org/10.1175/2008jamc1799.1.

Xu, M., C. Zhao, J. Gu, et al. 2021. "Convection-Permitting Hindcasting of Diurnal Variation of Mei-Yu Rainfall Over East China With a Global Variable-Resolution Model." *Journal of Geophysical Research: Atmospheres* 126, no. 14: e2021JD034823. https://doi.org/10.1029/2021JD034823.

Supporting Information

Additional supporting information can be found online in the Supporting Information section.